Korean J. Chem. Eng., **26**(2), 475-484 (2009)

Numerical and experimental investigation on a new modified valve in a valve tray column

Asghar Alizadehdakhel*, Masoud Rahimi*,†, and Ammar Abdulaziz Alsairafi**

*CFD Research Center, Chemical Engineering Department, Razi University, Kermanshah, Iran
**Faculty of Mechanical Engineering, College of Engineering and Petroleum, Kuwait University, Kuwait
(*Received 18 July 2008 • accepted 25 September 2008*)

Abstract–This paper reports experimental and computational fluid dynamics (CFD) modeling studies on the performance of three modified valves operating in a valve tray column. The original and modified valves including v-notched, warped and double-valve are tested experimentally. The experimental rig was a Perspex column having a single valve equipped with a fluctuating plate to measure the quality of gas distribution by using laser sensors. Two-stage nested designs were employed to show the repeatability and consistency of the measurements. In the CFD modeling, the volume of fluid (VOF) method was used to model the gas-liquid two-phase flow inside the column. A good agreement was observed between experimental data and the CFD predictions. The results showed that the double-valve layout provides a better gas distribution, smaller bubbles with greater interface area and lower pressure drop in comparison with the original and the two other modified valves.

Key words: Valve Tray, CFD, Hydrodynamics, Multiphase Flow, Bubble

INTRODUCTION

Gas/liquid contact is very important in most chemical industry equipment. Many investigations have been conducted to illustrate the effect of contact pattern on flow characteristics [1] and mass transfer rate [2]. Valve trays are popular gas-liquid contactors in the chemical process industries because of their flexibility in handling a wide range of vapor throughputs. In addition, valve trays exhibit a higher average operating efficiency than sieve trays which had been in use before [3]. Due to their common use in industries, even small modifications in their efficiency will cause huge economical benefits. Numerous investigations have been carried out for understanding the parameters that are effective on the tray efficiency.

Kozio and Kowiak [4] presented a dimensionless correlation for calculating the liquid entrainment of trays operating in the spray regime. They argued that their correlation is generally valid for all types of trays such as sieve, bubble cup, valve, tunnel, and cross-flow trays equipped with downcomers. Their correlation validity was confirmed on systems with different physical properties. Chang et al. [5] performed a dynamic simulation to find optimal operating conditions of a crude distillation unit. Their model included the mass and energy balance equations together with nonlinear equations for valve tray rating parameters describing the fluid behavior in the column such as downcomer load, jet flooding, hole velocity limit and downcomer backup. By solving the differential algebraic equations, they simulated the dynamic behavior of the unit during the startup and shutdown procedure. A model was developed by Wijn [6] for predicting the lower operating gas flow rate limits of distillation and absorption trays. The presented model included the simultaneous solution of two different liquid height equations. The first one was a common equation for normal tray operation, and the second one was a new equation describing the liquid height on a tray without downcomers. His model gave the liquid height and weep fraction as a function of gas and liquid flow rates for a given tray layout. The model was able to predict the gas flow rate at the weep and seal point in sieve and valve trays. He claimed that use of the weep point as a lower gas flow limit in sieve and valve trays can be replaced by a condition close to the seal point. An improved model of tray hydraulics was presented by Betlem et al. [7] over a broad operating range. The column dynamics was related to tray column design parameters and operating conditions. Consequently, they fitted the model parameters with column residence time measurements. In their study, two tray load regimes, an aeration regime and an obstruction regime, were distinguished. In addition, they studied the influence of the vapor flow on the column hydrodynamics. Wijn [8] described the mechanisms for liquid flow over outlet weirs of distillation and absorption trays. He proposed a new equation for estimating the liquid height on the tray that was a modification on the Francis weir equation, in which the effect of edge-vortex in the calming zone was included. Jacimovic [9] improved a one-parametric diffusion model to evaluate the effect of entrainment and mass transfer in the settling zone on the efficiency in tray columns. He reported that his model improves the accuracy of predicted mass transfer parameters including overall point efficiency, Peclet number and Murphree tray efficiency in the presence of entrainment. Rao et al. [10] used the direct incorporation of the efficiency matrix in the Naphtali Sandholm [11] method. They reported that their modified method has better convergence characteristics in comparison with the original Naphtali Sandholm method for distillation, absorption and extraction columns. The tray efficiency matrix used in their simulation was obtained from a point efficiency matrix.

Numerous investigations have been done to simulate and design distillation columns [12]. The hydrodynamics of gas and liquid flow on the tray has a significant effect on its efficiency [13]. The results obtained from computational fluid dynamics (CFD) modeling con-

†To whom correspondence should be addressed.
E-mail: masoudrahimi@yahoo.com

tain detailed information about the velocity, pressure, phase and component distributions inside the calculation domain. Therefore, CFD modeling of tray columns gives this opportunity to have a good understanding from the fluid hydrodynamics in this type of equipment. Recently, with the improvement of computer hardware and software and consequent increasing of the calculation speed, many studies have been carried out to model the fluid hydrodynamics in gas/liquid contactors using CFD modeling techniques.

The two-phase flow behavior on a sieve tray column using a two-dimensional model was studied by Yu et al. [14]. Their study focused on the description of the hydrodynamics along the liquid flow path. In that study, the variations in the gas flow direction along the height of the dispersion were ignored.

Van Batten and Krishna [15] developed a CFD model for describing the hydrodynamics of sieve trays. They modeled the gas and liquid phases in the Eulerian framework as two interpenetrating phases. The interphase momentum exchange coefficient was estimated based on the Bennett et al. [16] correlation. They reported that the predicted clear liquid height obtained from their modeling is in a good agreement with the Bennett correlation.

A CFD modeling was carried out by Van Baten et al. [17] to model the transient gas/liquid hydrodynamics on a sieve tray column. In their study, envelopes of catalyst were disposed along the liquid flow direction. Their CFD simulation work focused on the clear liquid height. They did some experiments to determine the clear liquid height on the tray as a function of tray geometry and operating conditions, and finally suggested that CFD modeling can be used for design and scale-up purposes.

Gesit et al. [18] employed the commercial CFX package to predict the flow patterns and hydraulics of a commercial scale 1.22 m diameter air/water sieve tray. In their investigation, the velocity distributions, clear liquid height, froth height and liquid holdup fraction in froth were predicted for various combinations of gas and liquid flow rates. Each phase was treated as an interpenetrating continuum having separate transport equations and interaction between them was considered via an interphase momentum transfer. They claimed that CFD can be used as a valuable tool in trays design and analysis.

Sun et al. [19] proposed a computational mass transfer (CMT) model to predict the turbulent mass transfer diffusivity and concentration profile on a tray as well as the tray efficiency of a distillation column. They showed that their simplified models can give better predictions on the turbulent mass transfer diffusivity than the original one as they compared the predicted results with the experimental data obtained from literature for an industrial scale distillation column. They reported that the computed concentrations at the outlet of each tray and the tray efficiency by these two models are in satisfactory agreement.

In recent research, Noriler et al. [20] applied a CFD model under an Eulerian-Eulerian framework for gas-liquid flows, with the capability of predicting the momentum/thermal behavior of the multiphase flows. They predicted volume fractions, velocities, pressure and temperature fields of two-phase flows on a sieve tray distillation. The authors illustrated the velocities, temperature as well as the volume fractions profiles as a function of the time and position in the distillation sieve tray.

In contrast with the importance and common use of valve tray columns, due to the complex geometry of their valves, limited numerical modeling was done to model the gas/liquid contact patterns on them [21].

In the present study, an experimental analysis and a three-dimensional CFD modeling were carried out to investigate the effect of the valve shape on gas dispersion quality inside a valve tray column. In this work, three different modifications were done on a valve which was employed in an industrial stripping column. The quality of the gas dispersion upon the tray using these valves has been investigated experimentally and theoretically.

EXPERIMENTAL WORK

An experimental column containing a valve tray was constructed to investigate gas/liquid hydrodynamics inside the column and the effect of valve shape on the tray performance. Modifications were done on a valve which was used in the stripping column of the catalytic reforming unit of Abadan Refinery of Iran. This valve was used as the basic valve and three different modifications were done on its shape to improve the tray efficiency. Small pieces from lead were stuck to the valves to equalize their weights. An attempt was made to change the shape of the valve in a way that breaks the bubbles into smaller sizes, because this increases the gas/liquid contact area.

The original and modified valves including v-notched, warped and double-valve are shown in Fig. 1. As can be seen, in the v-notched the valve edge was cut in a way that v-shaped edges were formed. The sharp edges created in this valve were supposed to break down the rising bubbles into smaller sizes. In the warped valve, the valve border was cut and screwed. It was realized that the screwed edges cause a tangential rotation in the gas flow. Therefore, the horizontal dispersion of gas and consequently the gas/liquid interface area were expected to be increased. In the last modification, a smaller valve

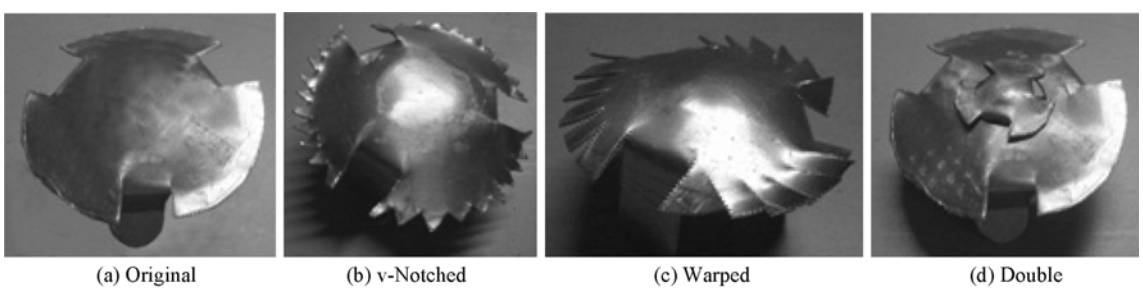

Fig. 1. The original and modified valves.

was placed upon the original one to construct the double-valve geometry. It was expected that in this layout the gas stream disperses in a more efficient way, because it divides into two portions as passing through two valves in series. In addition, at low gas flow rates it was realized that the upper valve can be opened while the lower one is closed. Therefore, the liquid weeping at low gas flow rates can be expected to be reduced.

A novel method was used to investigate the gas/liquid contact pattern established by different valves. Since different gas/liquid contact regimes cause different fluid momentum distribution upon the tray, the way that the liquid surface fluctuates should have significant differences. Therefore, for studying this matter, a fluctuating plate with a hinge to move in upward/downward directions was installed at a height of 8.5 cm above the tray. The oscillation frequency of movement of this plate, which is a criterion for the variations of the upward momentum acting on the plate, was measured by using laser emitter/receivers. Three pairs of laser emitter/receivers were installed at heights of 8.5, 9.5 and 10.5 cm from the tray. The received laser signals were sent to a digital counter that recorded the number of disconnections between emitter and receivers caused by the fluctuating plate. In fact, the intensity of fluctuating represents the size of bubbles inside the liquid phase. Larger bubbles, which are formed in weak gas distributions, cause the liquid surface to fluctuate stronger and the counter records larger numbers. On the other hand, smaller bubbles created in better gas distributions cause a calm liquid surface and the counter records smaller numbers. The experimental column, fluctuating plate and the laser emitter/receivers are shown in Fig. 2.

The liquid flow was chosen in such a way that the velocity of liquid upon the tray was approximately equal to the established liquid velocity on the trays of the industrial stripping column mentioned before. Also, the linear gas velocity going through the valve was the same as in the actual industrial setup. Therefore, values of 6 and 170 lit/min were used for the liquid and gas flow rates, respectively.

Each measurement was carried out during three 5-second intervals after the system reached steady state. To check the experimental work's repeatability, each experiment was repeated three times. Table 1 shows the recorded number of disconnections between emit-

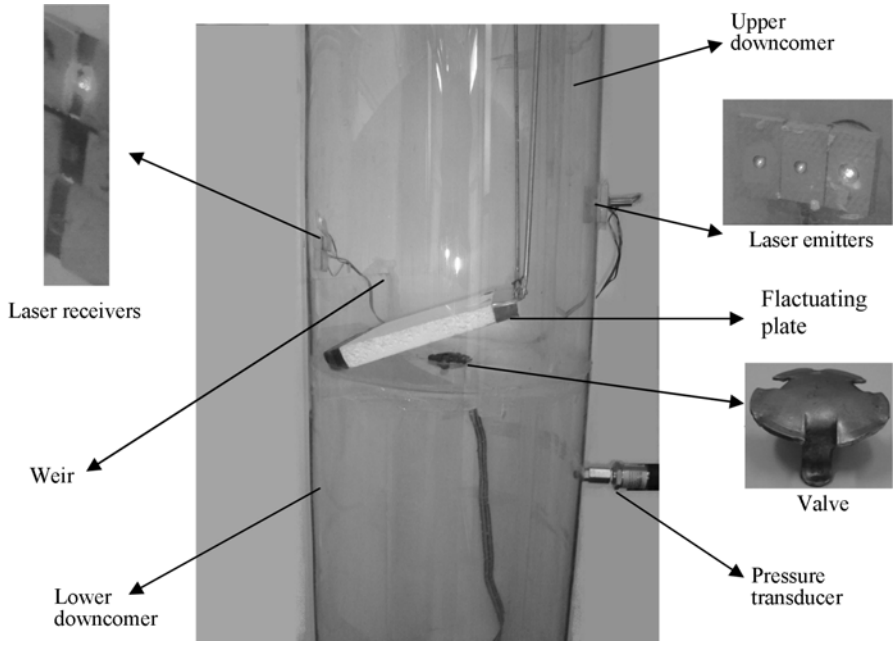

Fig. 2. The rig and its components.

Table 1. The number of disconnections and the calculated FN numbers

	Intervals	Original valve				v-Notched valve				Warped valve				Double valve			
		D1	D2	D3	FN	D1	D2	D3	FN	D1	D2	D3	FN	D1	D2	D3	FN
Exp 1	1	31	16	3	72	31	11	3	62	27	8	0	43	26	3	0	32
	2	30	14	4	70	25	4	7	54	29	3	1	38	28	5	0	38
	3	31	16	4	75	28	6	5	55	29	8	1	48	27	2	1	34
Exp 2	1	26	10	7	67	31	7	6	63	31	5	2	47	26	2	2	36
	2	31	11	8	77	31	6	5	58	25	3	3	40	23	2	1	30
	3	29	5	11	72	25	11	5	62	34	3	3	49	26	4	0	34
Exp 3	1	30	12	6	72	30	7	4	56	28	3	3	43	26	5	0	36
	2	27	9	10	75	29	3	9	62	30	1	5	47	27	5	1	40
	3	30	10	7	71	29	4	6	55	27	3	4	45	24	5	1	37

ter/receiver pairs caused by the fluctuating plate. D1, D2 and D3 are the number of disconnections for receivers 1, 2 and 3, respectively. In each experiment, the disconnection numbers were recorded during three 5-second intervals. When the first receiver counts a number, D_1, it means that only the path between emitter and receiver1 is disconnected. Recording a number on the second receiver, D_2, means that the plate obscures both the first and second receivers. Finally, as the third receiver counts a number, D_3, none of the receivers can see the emitters. Therefore, a frequency number (FN) can be defined as follows:

$$FN=D_1+2*D_2+3*D_3 \quad (1)$$

Where, FN is a criterion for showing the oscillation frequency of the fluctuating plate. The calculated FN values for the obtained disconnection numbers are given in Table 1.

Two-stage nested designs [22] were used to analyze the effect of the valve shape on the FN and the experiment's repeatability. The linear statistical model for the two-stage nested design is:

$$y_{ijk}=\mu+\tau_i+\beta_{j(i)}+\varepsilon_{(ij)k}\begin{cases} i=1,2,\ldots,a \\ j=1,2,\ldots,b \\ k=1,2,\ldots,n \end{cases} \quad (2)$$

Where, y_{ijk} are the observations or measurements and μ is the overall mean of the measurements. There are **a** levels of factor A, **b** levels of factor B nested under each level of A, and **n** replicates. The subscript j(i) indicates that the j^{th} level of factor B is nested under the i^{th} level of factor A. It is convenient to think of the replicates as being nested within the combination of levels of A and B; thus, the subscript (ij)k is used for the error term. This is a balanced nested design because there are an equal number of levels of B within each level of A and an equal number of replicates. Because every level of factor B does not appear with every level of factor A, there can be no interaction between A and B. As this is the case in this work, if A is a fixed factor and B is random, then H_o: $\tau_i=0$ is tested by MSA/MSB(A) and H_o: $\sigma_\beta^2=0$ is tested by MSB(A)/MSE. The analysis of variance for the two-stage nested design will be as in Table 2.

The valves were compared pair to pair to check the sequence of performance expected from designing their geometries. Therefore, three sets of two-staged nested designs were used. The first set compares the performance of the basic valve with the v-notched, the second one compares the v-notched with the warped valve, and the last set of designs was used to compare the warped with the double-valve. As an example, the two-stage nested design for comparing the FN values of the basic and v-notched valves is shown in Fig. 3.

Table 2. Analysis of variance table for the two-stage nested design

Source of variation	Sum of squares	Degree of freedom	Mean square
A	$\frac{1}{bn}\sum_{i=1}^{a} y_{i..}^2 - \frac{y_{...}^2}{abn}$	a−1	MSA
B within A	$\frac{1}{n}\sum_{i=1}^{a}\sum_{j=1}^{b} y_{ij.}^2 - \frac{1}{bn}\sum_{i=1}^{a} y_{i..}^2$	a(b−1)	MSB(A)
Error	$\sum_{i=1}^{a}\sum_{j=1}^{b}\sum_{k=1}^{n} y_{ijk}^2 - \frac{1}{n}\sum_{i=1}^{a}\sum_{j=1}^{b} y_{ij.}^2$	ab(n−1)	MSE
Total	$\sum_{i=1}^{a}\sum_{j=1}^{b}\sum_{k=1}^{n} y_{ijk}^2 - \frac{y_{...}^2}{abn}$	abn−1	

The analysis of variance for the three set of designs is given in Table 3. The calculated F-values were compared to one-tailed F-value obtained from F-tables [23]. In this method, if the calculated F-value for the valve effect (i.e., the ratio of valve's mean of square to the experiment's mean of square) is greater than one-tailed F-value read from F-Table, it means that the FN obtained from one valve (the one that is expected to be better) is significantly smaller than that of the other valve. In addition, the degree of confidence depends on the F-value chosen from F-Tables. For checking the repeatability of the experiments, it should be checked whether the FN obtained for a valve at constant conditions and different time intervals are different or not. Therefore, two-tailed F-values should be used. If the calculated F-value for the experiments effect (i.e., the ratio of the experiment's mean of square to the error's mean of square) is greater than two-tailed F-value read from F-Table, it means that the effect of repeating the experiments is significant.

From the F-table, the one-tailed F-value for $\varphi_{1,4}$ with 99.9% degree

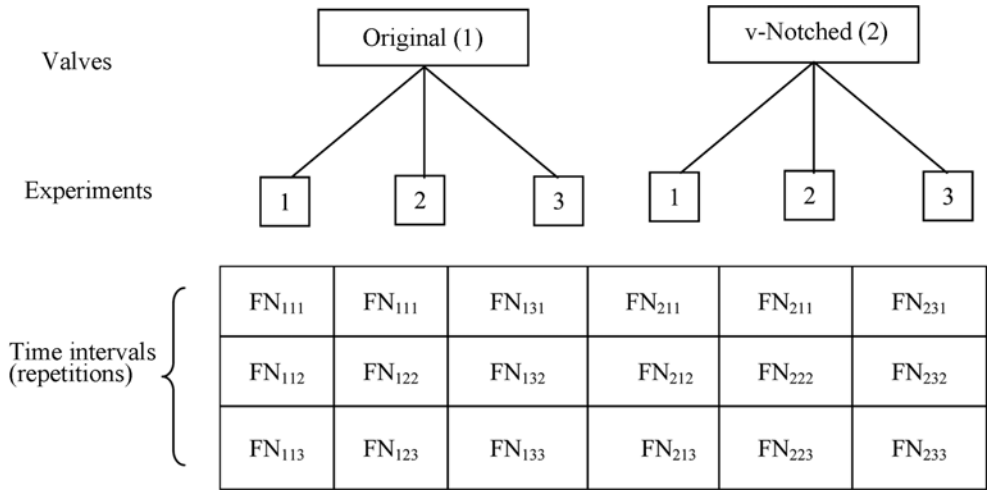

Fig. 3. Two-stage nested design for comparing the function of original and v-notched valves.

Table 3. Analysis of variance for the three set of designs

	Source of variation	Sum of sq.	Degree of freedom	Mean square	F0
Original and v-notched	Valves	854.2	1	854.2	121.1
	Experiments	28.2	4	7.1	0.56
	Error	152	12	12.7	
	Total	1034.4	17		
v-Notched and warped	Valves	896.1	1	896.1	96.6
	Experiments	37.1	4	9.3	0.61
	Error	183.3	12	15.3	
	Total	1116.5	17		
Warped and double	Valves	460.1	1	460.1	129.4
	Experiments	14.2	4	3.6	0.20
	Error	218	12	18.2	
	Total	692.3	17		

of confidence is 74.14. From Table 3, the calculated F-value for the difference between basic and v-notched valve is 121.1. Also, the values of 96.6 and 129.4 were obtained for the difference between v-notched/warped and warped/double-valve layouts, respectively. Since all the calculated F-values for the effect of the valve shape are bigger than the F-value presented in the F-table, the effect of the valve shape in all cases is highly significant and there is a sequence between the FN values as follows:

$$FN_{original}>FN_{v\text{-}notched}>FN_{warped}>FN_{double\text{-}valve}$$

In addition, the two-tailed F-value for $\varphi_{4,12}$ with 95% degree of confidence is 4.12, and it can be seen from Table 3 that the calculated F-value for the experiment effect in all cases is smaller than 4.12. Therefore, the effects of errors in the experiments were negligible, i.e., the experiments were repeatable and there was consistency in the measured results.

The greater numbers of FN means that the fluctuating plate undergoes more oscillation. Therefore, the experimental results show that the oscillation frequency of the fluctuating plate had the following sequence:

original>v-notched>warped>double-valve

A lower oscillation frequency of the fluctuating plate means that the gas bubbles produced inside the liquid phase by that valve were smaller and better gas distribution occurred. Therefore, the double-valve layout which caused the lowest oscillation frequency had the best gas distribution in comparison with the other examined valves.

CFD MODELING

The commercial CFD package FLUENT6.2 was used to model the gas-liquid motions in the experimental column in order to investigate the effect of the valve shape on gas dispersion quality on the tray. The interface between gas/liquid phases is important in evaluating the performance of the tray; therefore, free surface modeling is necessary. This is one of the challenging research areas for providing an efficient solver. Volume of fluid (VOF) [24] and Levelset [25] approaches belong to the two best possible implicit free surface reconstruction methods, while, particularly, VOF is relatively simple to treat topological changes of the interface and is naturally conservative. In the present work, water and air were used as working fluids and the VOF model was employed. The VOF method relies on the fact that two or more phases are not interpenetrating and for each additional phase the volume fraction of the phase must be added in the computation. In the VOF model, the sum of the volume fractions of all phases in each control volume is equal to one. In the modeling, the incompressible Navier-Stokes equations for velocity, u, and pressure, p, are solved simultaneously. These equations are as follows [24]:

$$\text{Continuity:} \quad \nabla\cdot u=0 \tag{3}$$

$$\text{Momentum:} \quad \frac{\partial u}{\partial t}+\nabla\cdot(uu)=-\frac{1}{\rho}[\nabla p-\nabla\cdot(2\mu S)]+\frac{1}{\rho}F_{SF} \tag{4}$$

Where, F_{SF} is the continuum surface force (CSF) vector and S is the deformation tensor given as follows:

$$S=\frac{1}{2}(\nabla u+[\nabla u]^{T}) \tag{5}$$

In Eq. (4), the density (ρ) and viscosity (μ) of the fluid depend on the volume fractions of each phase and are calculated by the following equations:

$$\rho=\alpha\rho_{air}+(1-\alpha)\rho_{water} \tag{6}$$

$$\mu=\frac{\alpha\rho_{air}\mu_{air}+(1-\alpha)\rho_{water}\mu_{water}}{\alpha\rho_{air}+(1-\alpha)\rho_{water}} \tag{7}$$

Where, α is the air volume fraction in the cell. The interface between two phases was tracked by the volume fraction. Conservation of α can be represented by the interface mass balance by using the following equation:

$$\frac{\partial\alpha}{\partial t}+u\cdot\nabla\alpha=0 \tag{8}$$

The cell phase is gas where α=1, while α=0 means that the whole volume has been occupied by the liquid. It can be concluded that the gas/liquid interface exists in the regions that α lies between zero and one.

1. Mesh Geometry

In the pre-processing part of the CFD modeling, the domain was divided into small control volumes using tetrahedral cells. An investigation was done on the predicted gas/liquid interface area to find the optimum grid size. Three different sizes of grid were used to mesh the column containing the basic valve, and the predicted gas/liquid interface areas using these layouts were compared. Values of 0.1556, 0.1794 and 0.1808 m^2 interface areas were obtained as the domain was meshed into 110048, 713729 and 2124327, respectively. Therefore, increasing the number of control volumes from 110048 to 713729 caused a significant difference in the predicted interface area. However, employing a greater number of control volumes than 713729 showed only a negligible difference in the calculated contact areas. Thus, the second mesh layout was chosen as the optimum size of the control volumes. In this study, the same sizes of grids were used to mesh the column containing modified valves. Fig. 4 shows the triangle mesh layouts on surface of the four studied valves. The created grids in a vertical slice of the column containing the double-valve geometry are shown in Fig. 5. As illus-

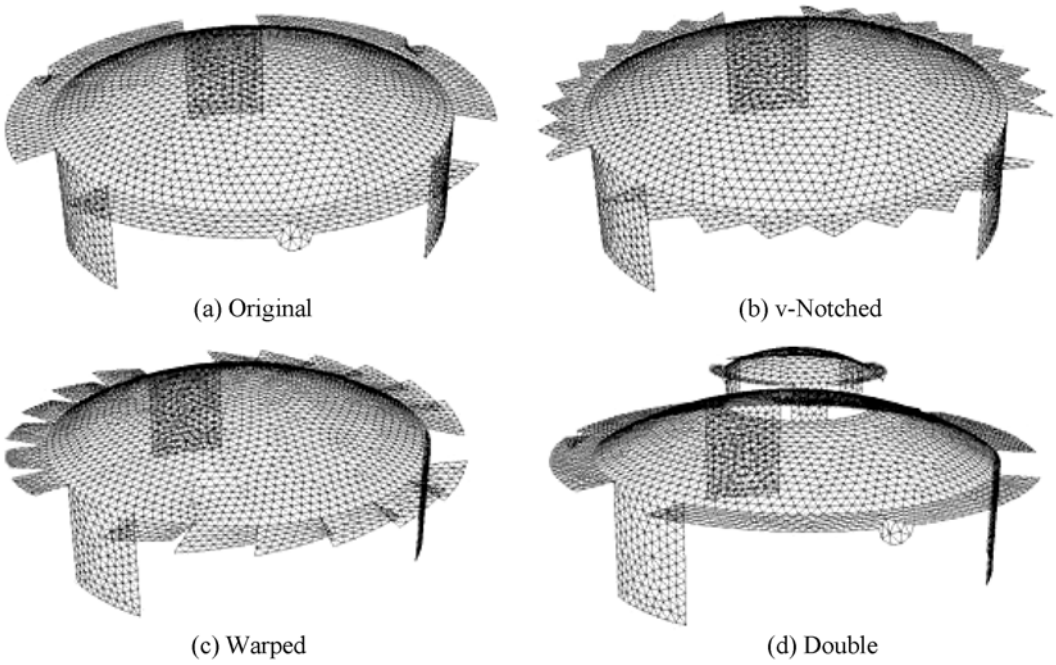

Fig. 4. The meshed configuration on the valve surface.

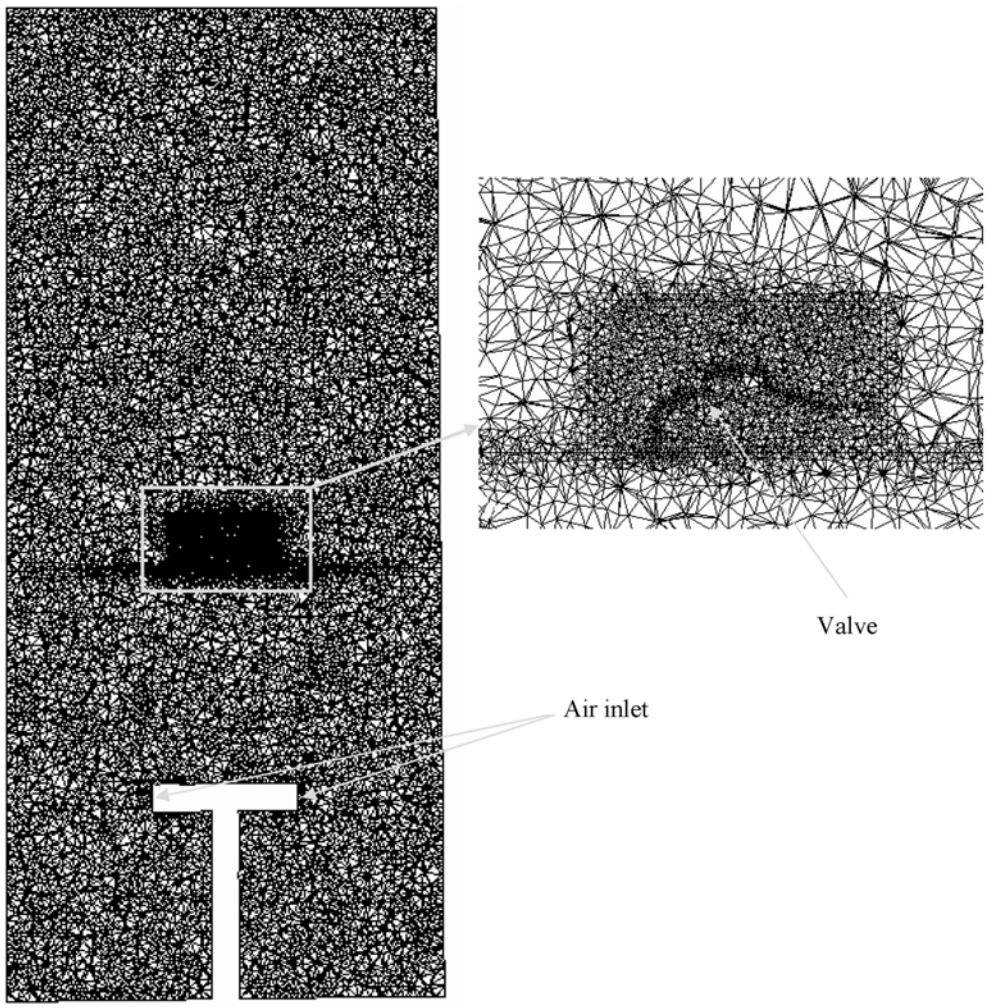

Fig. 5. A view of the meshed column in a vertical slice.

trated in the figure, different mesh sizes were used in different places of the modeling domain. Finer meshes were used near the valve, which is the main region for the gas-liquid contact.

2. Initial and Boundary Conditions

Despite the fixed values of the gas and liquid flow rates, the modeling was carried out in unsteady state for tracking the shape and place of gas/liquid interface (i.e., the boundaries of gas bubbles and the free surface) with time. In all cases, first order unsteady state calculations were done by using 0.0001 s time steps. A mass flow rate of 0.1 kg/s was applied for the liquid inlet and a velocity inlet of 5 m/s (170 lit/min) was used for the gas stream. In addition, atmospheric pressure was set at outlet of the column. Similar to the experiments, the initial volume fraction of water was set to one on the tray up to the weir height (8 cm) and zero in the other regions. No outlet stream was considered for the liquid phase and let the water move downward and accumulate in the bottom of the column the same as in the experiments. For the gas inlet, a gauge inlet pressure of 800 Pa was used as boundary condition for all valves. Since the employed experimental fluctuating plate was very light in weight, it was assumed that it had no effect on the fluid surface oscillation. Therefore, the liquid surface above the tray was considered as a free surface in the modeling. This was done in order to reduce the computational time of moving wall complicated modeling. In addition, because the experimental pressure fluctuation in the experiment was negligible, it was assumed that the valves were completely open and did not move during the operation. The assumptions significantly reduced the computational time.

RESULTS AND DISCUSSION

Fig. 6 shows the predicted contour plot of the liquid phase volume fraction for the original valve in a vertical slice inside the column. According to the figure, liquid moves downward from the inlet and pours on the tray. The gas goes upward from the tray hole and splashes the liquid phase into the air. The liquid stream passes through the weir and flows downward via the downcomer. Due to higher pressure established under the tray, water collects in a height pro-

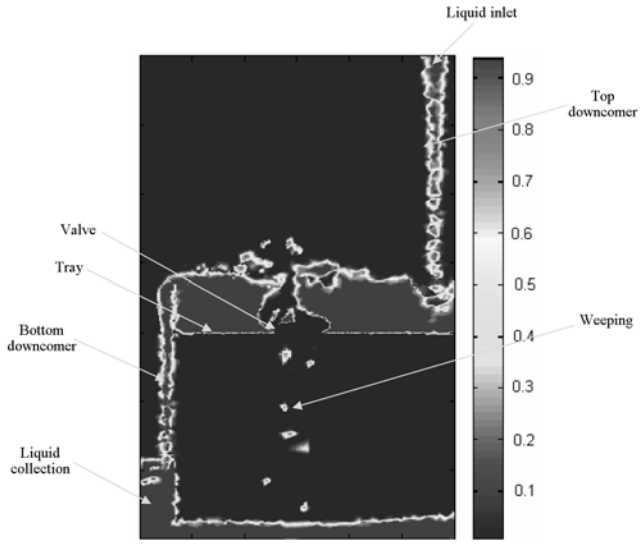

Fig. 6. Contour plot of the liquid volume fraction in a vertical slice.

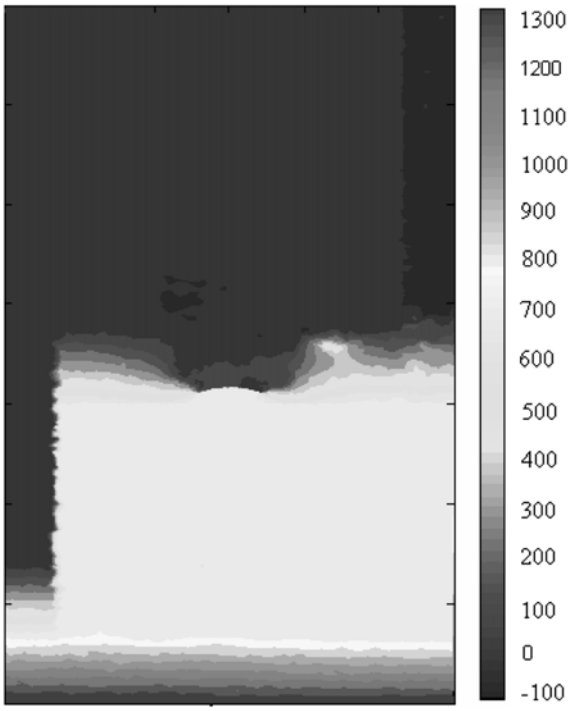

Fig. 7. Predicted pressure distribution in the column (Pa) for the original valve.

portional to this pressure inside the downcomer. In addition, in this figure, it is possible to see the liquid weeping below the tray.

An example of the pressure field contour plot of the above-mentioned slice for the original valve is illustrated in Fig. 7. The figure shows that pressure in the gas region below the tray is approximately constant. There is a gradual change in the pressure on the tray due to the liquid weight except in the regions close to the valve, where a sharp pressure drop took place due to the blocking effect of the valve. This causes the air bubbles to collapse and divert to the lateral sides. The negative pressures established at the liquid inlet section, where the liquid falls down, can be explained by the gravity effect. Finally, at the top region of the column the atmospheric pressure, which was set in the model boundary conditions, is observable.

The velocity vectors for v-notched and warped valves in a horizontal plane above the valves are compared in Fig. 8. The figure shows that the special geometry of the warped valve causes a tangential rotation in the flow pattern, while in the v-notched valve only radial velocities can be observed. To follow the gas velocity on the valve region more quantitatively, the velocity at an imaginary ring with 2.2 and 3 cm inner-outer diameters just above the valve was calculated for each case. The results showed that the average horizontal velocities for the warped and v-notched valves are 1.64 and 1.26 m/s, respectively. In addition, the average upward velocities in this ring are 2.08 and 2.64 for the warped and v-notched valves. It means that for the warped valve, the gas leaving the valve tends to flow tangentially, which causes a greater contact time between the gas and liquid. However, as the v-notched valve was employed, the gas bubbles have bigger upward velocities, spend less time in the liquid phase and consequently provide less contact time.

Fig. 9 shows the velocity vectors on a vertical plane going through the double-valve. It can be seen that the gas flow leaving the hole

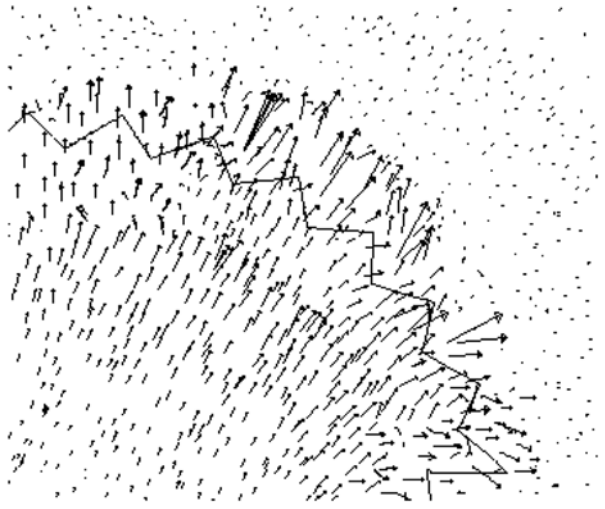

(a) v-Notched

(b) Warped

Fig. 8. Velocity vectors in a horizontal slice 1 mm above the valve border.

is divided to two separate streams. A part of the gas enters the liquid phase below the lower cap and the rest of it finds its way through the valve hole. This causes the gas bubbles to break down into smaller bubbles and provide more contact areas.

The predicted gas/liquid contact area was used to compare the performance of the valves on the tray. As mentioned before, a gas/liquid interface exists in places that the volume fraction of gas, α, lies between zero and one. Different values of α were used as the criterion for the location of the interface, and the area of the interface in each case was calculated. The calculated gas/liquid interface areas for the four valves using various values of α are given in Fig. 10. The figure shows that the provided interface areas in all of the modified valves are greater than the original one. This was obtained due to the formation of smaller bubbles that were completely described before. However, in the double-valve layout dividing of the gas stream into two passages had a more significant effect on creating smaller bubbles and greater contact area. Hence, the overall survey shows that the double-valve layout works in a more efficient way in comparison with the original and other modified valves.

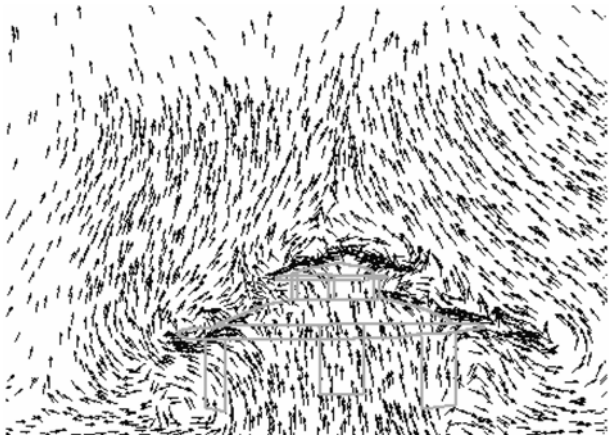

Fig. 9. Velocity vectors on a vertical plane that goes through the double-valve.

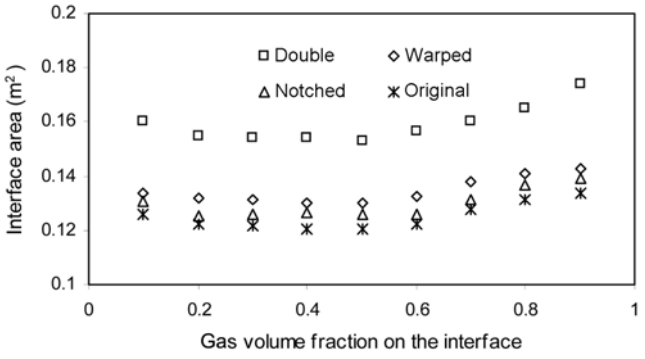

Fig. 10. The calculated gas-liquid interface areas (m^2) using various gas volume fraction criteria.

Table 4. Comparison between the predicted and measured pressure drops

	Experimental (Pa)	Predicted (Pa)	Error %
Original	753	747	0.80
Notched	749	744	0.67
Warped	758	752	0.79
Double	693	687	0.87

The experimental and CFD predicted pressure drops for different valves are presented in Table 4. The table shows that the predicted tray pressure drops are quite close to the measured ones. In addition, the pressure drops for different valves are almost the same, except for the double-valve layout that is about 8% less than the others.

We used another way to compare the CFD predictions with experimental measurements. In this method the predicted momentum acting on the fluctuating plate, which causes the plate oscillations, was related to the measured FN values. From the theoretical point of view, the fluctuating plate moves upward due to momentum transfer from the fluid to the plate. The momentum per unit volume of fluid in the vertical direction can be calculated with multiplying the fluid density by the vertical velocity, u_y, as follows:

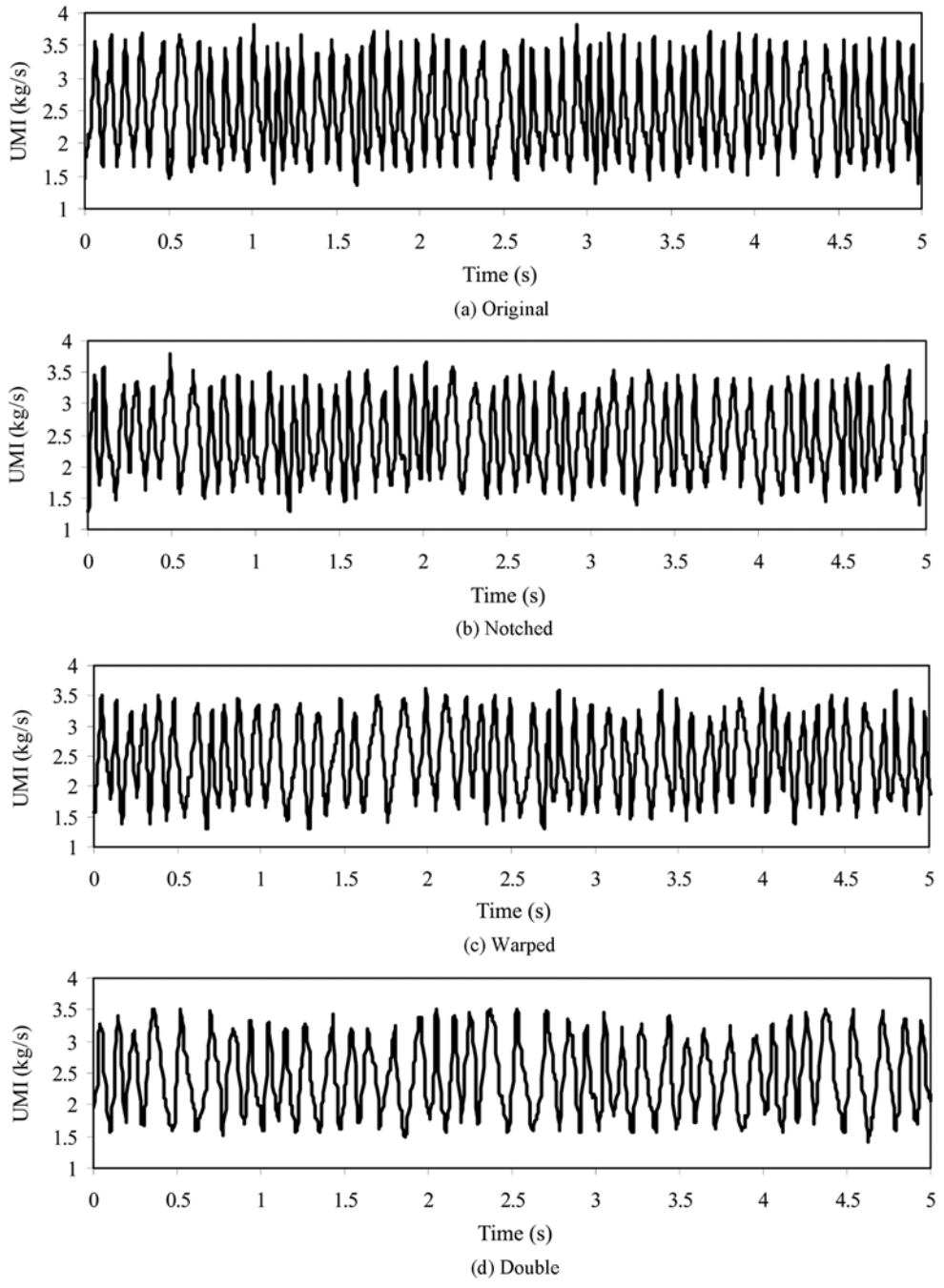

Fig. 11. The predicted variations of the UMI on the fluctuating plate for different valves.

$$\textit{vertical momentum per unit volume} = \rho u_y \tag{9}$$

Since only the upward component of momentum can affect the upward movement of the fluctuating plate, it is possible to define the upward momentum as follows:

$$\textit{upward momentum per unit volume} = \rho\left(\frac{u_y + \mathrm{abs}(u_y)}{2}\right) \tag{10}$$

The integral of this parameter over the whole surface of an imaginary horizontal plate, located at the same height of the fluctuating plate, gives the upward momentum integral per unit volume of the fluid (UMI) acting on the fluctuating plate as follows:

$$\mathrm{UMI} = \int_A \rho\left(\frac{u_y + \mathrm{abs}(u_y)}{2}\right) dA \tag{11}$$

Fig. 11 shows the variations of the CFD predicted UMI at various time steps for the original and modified valves. The figure shows that the UMI has about 56, 53, 50, and 40 cycles for the original, notched, warped and double-valve layouts, respectively. In the other words, the frequency of UMI variation has a similar trend as the FN, which was described in the experimental section. The frequency of UMI variations (i.e., number of fluctuations with time) is proportional to the FN number. Lower values mean better gas distribution in the liquid phase. The observed trend can be explained by

the fact that the better valves provide smaller bubbles, a more homogeneous gas distribution and consequently less oscillation of the fluctuating plate. Therefore, the double-valve geometry should work in a more efficient way in comparison with the other ones.

In summary, CFD is a powerful tool to model pressure drop and gas/liquid interface of two-phase flow in valve tray columns. In addition, applying the modified double-valve geometry presented in this investigation will result in a lower pressure drop, better gas distribution in the liquid, and greater gas-liquid contact area in comparison with the original one. Trays equipped with this type of valve are expected to operate in a more efficient way in separation columns.

CONCLUSION

A new modified double-valve has been introduced. This research shows that the double-valve layout creates a higher contact area and a lower pressure drop in comparison with the original and two other modified valves, v-notched and warped ones. In addition, a simple and low cost experimental method was successfully applied to evaluate the gas/liquid contact pattern using a fluctuating plate and laser beams. Two-stage nested designs were employed to show the repeatability and consistency of the measurements. A CFD predicted parameter, UMI, was defined for evaluating the valves' performance. Although the UMI has no specific meaning in mass transfer by itself, the frequency of its changes represents the quality of gas distribution in the liquid phase. This is very important from the mass transfer point of view. Higher quality of gas distribution in a liquid gives more surface for mass transfer and consequently increases the mass transfer rate. The lower values of UMI fluctuation show lower value of momentum transfer to the plate and better distribution of gas in liquid and vice versa. Therefore, it is possible to say practically that a system which works with lower frequency of change in UMI may cause higher mass transfer rate.

NOMENCLATURE

D : number of disconnection between laser beam pairs
F_N : frequency number
F_{SF} : continuum surface force vector [Nm^{-3}]
P : pressure [Pa]
S : ceformation tensor [s^{-1}]
t : time [s]
u : velocity vector [m s^{-1}]
u_y : vertical velocity component [m s^{-1}]
UMI : upward momentum integral per unit volume [kg s^{-1}]

Greek Letters

α : air volume fraction
μ : viscosity [Pa s]
ρ : density [kg m^{-3}]

REFERENCES

1. M. Ide, H. Uchiyama and T. Ishikura, *Korean J. Chem. Eng*., **16**, 698 (1999).
2. N. Tunthikul, P. Wongsuchoto and P. Pavasant, *Korean J. Chem. Eng*., **23**, 881 (2006).
3. J. L. Peytavy, M. H. Huor and R. Bugarel, *Chem. Eng. Process*., **27**, 155 (1990).
4. A. Kozio and J. M. Kowiak, *Chem. Eng. Process*., **27**, 145 (1990).
5. B. Chang, S. Lee, H. Kwon and I. Moon, *Comput. Chem. Eng*., **22**, 863 (1998).
6. E. F. Wijn, *Chem. Eng. J*., **70**, 143 (1998).
7. B. H. L. Betlem, J. E. Rijnsdorp and R. F. Azink, *Chem. Eng. Sci*., **53**, 3991 (1998).
8. E. F. Wijn, *Chem. Eng. J*., **73**, 191 (1999).
9. B. M. Jacimovic, *Chem. Eng. Sci*., **55**, 3941 (2000).
10. D. P. Rao, C. V. Goutami and S. Jain, *Comput. Chem. Eng*., **25**, 1141 (2001).
11. L. M. Naphtali and D. P. Sandholm, *AIChE J*., **17**, 148 (1971).
12. Y. H. Kim, K. S. Hwang and M. Nakaiwa, *Korean J. Chem. Eng*., **21**, 1098 (2004).
13. Z. Lei, Q. Li, C. Li and B. Chen, *Korean J. Chem. Eng*., **21**, 1003 (2004).
14. K. T. Yu, X. G. Yan, X. Y. You and C. J. Liu, *Chem. Eng. Res. Des*., **77**, 554 (1999).
15. J. M. Van Baten and R. Krishna, *Chem. Eng. J*., **77**, 143 (2000).
16. D. L. Bennett, R. Agrawal and P. J. Cook, *AIChE J*., **29**, 434 (1983).
17. J. M. Van Baten, J. Ellenberger and R. Krishna, *Catal. Today*, **66**, 233 (2001).
18. G. Gesit, K. Nandakumar and K. T. Chuang, *AIChE J*., **49**, 910 (2003).
19. Z. M. Sun, K. T. Yu, X. G. Yuan and C. J. Liu, *Chem. Eng. Sci*., **62**, 1839 (2007).
20. D. Noriler, H. F. Meier, A. A. C. Barros and M. R. Wolf Maciel, *Chem. Eng. J*., **136**, 133 (2008).
21. S. Pradhan and A. Kannan, *Korean J. Chem. Eng*., **22**, 441 (2005).
22. D. C. Montgomery, *Design and analysis of experiments*, John Wiley & Sons, New York (2001).
23. L. Davies, *Efficiency in research, development and production: the statistical design and analysis of chemical experiments*, Royal Society of Chemistry, Cambridge (1993).
24. C. W. Hirt and B. D. Nichols, *J. Comput. Phys*., **39**, 201 (1981).
25. M. Lappa, *J. Biomech*., **38**, 185 (2005).
26. Fluent Inc, Fluent 6.2 User's Guide (2005).